PHYSICAL REVIEW B **79**, 020403(R) (2009)

Giant magnetic anisotropy of the bulk antiferromagnets IrMn and $IrMn_3$ from first principles

L. Szunyogh,[1,*] B. Lazarovits,[1,2] L. Udvardi,[1] J. Jackson,[3] and U. Nowak[4]
[1]*Department of Theoretical Physics, Budapest University of Technology and Economics, Budafoki út 8, H1111 Budapest, Hungary*
[2]*Research Institute for Solid State Physics and Optics, Hungarian Academy of Sciences, P.O. Box 49, H-1525 Budapest, Hungary*
[3]*Department of Physics, University of York, York YO10 5DD, United Kingdom*
[4]*Fachbereich Physik, Universität Konstanz, 78457 Konstanz, Germany*
(Received 10 November 2008; published 13 January 2009)

We perform an *ab initio* study of the ordered phases of IrMn and $IrMn_3$, the most widely used industrial antiferromagnets. Calculation of the form and the strength of the magnetic anisotropy allows the construction of an effective spin model, which is tested against experimental measurements regarding the magnetic ground state and the Néel temperature. Our most challenging result is the extremely strong second-order anisotropy for $IrMn_3$ appearing in its frustrated triangular magnetic ground state, which is surprising since the ordered $L1_2$ phase has a cubic symmetry. We explain this large anisotropy by the fact that cubic symmetry is locally broken for each of the three Mn sublattices.

DOI: 10.1103/PhysRevB.79.020403 PACS number(s): 75.30.Gw, 75.50.Ss, 71.15.Mb, 71.15.Rf

Interest in the magnetic anisotropy (MA) of antiferromagnets comes from the fact that these compounds are important components of giant magnetoresistance (GMR) sensors used, e.g., in hard disk read heads. Antiferromagnetic (AF) materials are employed in these devices to form antiferromagnet/ferromagnet bilayers exhibiting exchange bias,[1] a shift of the hysteresis loop of the ferromagnet, providing a pinned layer which fixes the magnetization of the reference layer of a GMR sensor. The stability of the antiferromagnet is most crucial for the stability of exchange bias and hence the functioning of the device.[2,3] Industrially the antiferromagnet IrMn is widely used because of the large exchange bias and thermal stability that can be obtained with this material.

Recent estimates of the MA of IrMn have been concerned with the mean blocking temperature T_B, the temperature at which the exchange-bias shift changes sign upon thermal activation. From T_B the intrinsic MA can be estimated if the antiferromagnetic grain size distribution is known and if individual grains are assumed to be single domain, with the energy barrier to sublattice reversal given by the product of intrinsic anisotropy and grain volume, KV. Such a procedure has recently been reported and the room-temperature MA energy of IrMn was found to be 5.5×10^6 erg/cc (Ref. 4) and even 3.3×10^7 erg/cc,[5] depending on the seed layer upon which the IrMn films were grown and, consequently, the quality of the crystal ordering of the IrMn films. The largest MA was found for the sample displaying the highest degree of crystallographic order.

There are only a few first-principles calculations available in the literature related to relativistic effects in Mn-based antiferromagnets. It is shown that in the case of the frustrated antiferromagnet Mn_3Sn these effects can lead to the formation of weak ferromagnetism.[6] Umetsu *et al.*[7] calculated the magnetic anisotropy energy (MAE) of $L1_0$-type MnTM (TM=Ni, Pd, Pt, Rh, and Ir) compounds and revealed that MnIr has the highest MAE with a value of −7.05 meV/unit cell. Very recently, a MAE of 2.8 meV/unit cell was inferred for the low-temperature D phase of the $L1_2$-type Mn_3Pt alloy.[8]

In the present work, we address several features of the MA of IrMn alloys based on first principles. In terms of simple symmetry considerations, we predict the form of the MA energy that we fully confirm using *ab initio* calculations, which provide also the strength of the MA, i.e., the relevant MA constants.

Our most remarkable observation is the surprisingly strong second-order MA of $IrMn_3$ resulting from the fact that the cubic symmetry is locally broken for each of the three Mn sublattices. We are also able to attribute contributions of the MAE related to on-site and two-site exchange anisotropy terms, a very important issue for finite-temperature magnetism.[9,10] Such a separation is inevitably important for the purpose of subsequent simulations to study exchange-bias systems based on these compounds, for example, in determining the scaling behavior of the MA energy.

Self-consistent calculations are performed in terms of the fully relativistic screened Korringa-Kohn-Rostoker (SKKR) method.[11] Within this method, spin-polarization and relativistic effects (in particular, spin-orbit coupling) are treated on equal theoretical footing by solving the Kohn-Sham-Dirac equation. The local spin-density approximation as parametrized by Vosko *et al.*[12] was applied. The effective potentials and fields were treated within the atomic sphere approximation with an angular momentum cutoff of $\ell_{\max}=2$. For the $L1_0$ IrMn alloy we used the lattice constants $a=3.855$ Å and $c=3.644$ Å,[13] while for the $L1_2$ $IrMn_3$ alloy an fcc lattice with $a=3.785$ Å was considered.[14,15] For the self-consistent calculations we fixed the orientations of the magnetic moments on the Mn atoms according to the magnetic ground-state configurations reported previously in the literature, namely, a checkerboard collinear AF structure for $L1_0$ IrMn (Refs. 13 and 16) and a triangular ($T1$) state within the fcc (111) planes for $L1_2$ $IrMn_3$.[14,15] We obtained vanishing spin polarization at the Ir sites, and spin magnetic moments of $2.63\mu_B$ and $2.66\mu_B$ at the Mn sites for IrMn and $IrMn_3$, respectively. These values are in satisfactory agreement with earlier first-principles calculations.[13,15]

We start our study of the MA by symmetry considerations based on the following effective spin Hamiltonian (energy per unit cell):

 ©2009 The American Physical Society

$$H = -\frac{1}{2}\sum_{a,b=1}^{n} J_{ab}\vec{S}_a\vec{S}_b - \frac{1}{2}\sum_{a,b=1}^{n} \vec{S}_a\boldsymbol{D}_{ab}\vec{S}_b - \sum_{a=1}^{n} \vec{S}_a\boldsymbol{K}_a\vec{S}_a, \quad (1)$$

where $\vec{S}_a$ is the spin vector of the Mn sublattice labeled by a; $n=2$ for $L1_0$ IrMn and $n=3$ for $L1_2$ $IrMn_3$. Note that in Eq. (1) only terms up to second order in the spin variables are considered, $\boldsymbol{D}_{ab}$ are (traceless) symmetric matrices representing anisotropic two-site (exchange) coupling, and $\boldsymbol{K}_a$ are the on-site anisotropy matrices.[17] All the parameters in Eq. (1) are defined as sums over sites in the sublattices, e.g., $J_{ab}=\Sigma_{j\in b}J_{ij}$ for $i\in a$ ($j=i$ excluded), J_{ij} being the isotropic intersite interactions. In the case of $L1_0$ IrMn, tetragonal symmetry implies

$$\boldsymbol{D}_{ab} = D_{ab}\begin{pmatrix} -\frac{1}{2} & 0 & 0 \\ 0 & -\frac{1}{2} & 0 \\ 0 & 0 & 1 \end{pmatrix}, \quad \boldsymbol{K}_a = K\begin{pmatrix} 0 & 0 & 0 \\ 0 & 0 & 0 \\ 0 & 0 & 1 \end{pmatrix}, \quad (2)$$

with $D_{11}=D_{22}=D$ and $D_{12}=D'$. Rotating an antiferromagnetic configuration around the (100) axis, $\vec{S}_1=(0,\sin\varphi,\cos\varphi)$ and $\vec{S}_2=-\vec{S}_1$, a simple orientation (φ–) dependence of the energy can be derived, $E(\varphi)=E(0)+K_{\text{eff}}\sin^2\varphi$, introducing an effective uniaxial MA constant per unit cell, $K_{\text{eff}}=2K+\frac{3}{2}(D'-D)$.

In order to calculate $E(\varphi)$ from first principles, we adopted the so-called *magnetic force theorem*[18] in which the previously determined self-consistent effective potentials and fields are kept fixed and the change in total energy of the system with respect to φ is approached by that of the single-particle (band) energy. The values for $E(\varphi)$ from these calculations could be very well fitted with $K_{\text{eff}}=-6.81$ meV, in very good agreement with the theoretical value reported by Umetsu *et al.*[7] and also with the easy-plane anisotropy observed experimentally.[16] Furthermore, by using the method described in Ref. 17 we calculated an on-site anisotropy constant of $K=-2.94$ meV. This result implies that in this system the MA energy is dominated by the on-site anisotropy, i.e., the third term in Eq. (1).

In the case of $L1_2$ $IrMn_3$, for each of the three Mn atoms in a unit cell a tetragonal symmetry axis of the lattice applies as indicated in Fig. 1. This *local* tetragonal symmetry generates again uniaxial two-site and on-site magnetic anisotropies, however, with different symmetry axes that have to be accounted for in Eq. (1) by suitable transformations of the matrices in Eq. (2). C_3 rotational symmetry around the (111) axes furthermore implies $D_{11}=D_{22}=D_{33}=D$ and $D_{12}=D_{23}=D_{31}=D'$. Clearly, for a ferromagnetic state of the system, such a Hamiltonian would yield a vanishing MA energy.

This second-order MA becomes, however, evident if all the spins forming the $T1$ ground state are rotated around the (111) axis. Straightforward calculations show that $E(\varphi)$ follows again a $\sin^2\varphi$ dependence with an effective MA constant $K_{\text{eff}}=2K+\frac{3}{2}(D+D')$. Our first-principles calculations reproduced well the proposed functional form of $E(\varphi)$ with a value of $K_{\text{eff}}=10.42$ meV; see Fig. 2. Thus we conclude that the MA constant for $L1_2$ is almost twice as large in magnitude than for $L1_0$ IrMn.

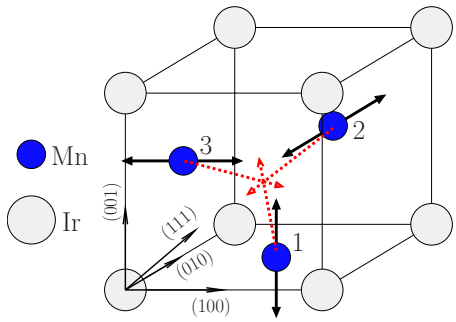

FIG. 1. (Color online) Sketch of the $IrMn_3$ unit cell. Dark spheres represent three Mn atoms corresponding to the antiferromagnetic sublattices. The solid arrows indicate the local easy axes and the dotted arrows indicate the spin direction in the $T1$ ground state.

We confirm the validity of spin Hamiltonian (1) for $L1_2$ $IrMn_3$ by applying two additional rotations of the spin system. First, we repeat the rotation around the (111) axis by simultaneously interchanging the orientations of the spins at Mn sites 2 and 3. It should be mentioned that this triangular spin structure (say, $T2$) corresponds to a chirality vector,

$$\vec{\kappa} = \frac{2}{3\sqrt{3}}(\vec{S}_1\times\vec{S}_2 + \vec{S}_2\times\vec{S}_3 + \vec{S}_3\times\vec{S}_1), \quad (3)$$

which is just the opposite of the chirality vector related to state $T1$. Note also that $\vec{\kappa}$ is normal to the plane of the moments and the normal component of this vector (chirality index) κ for state $T1$ is $\kappa=1$, while for state $T2$ $\kappa=-1$. While by considering only the first (isotropic) term in Eq. (1) the energy of these two states is identical, the anisotropy terms lift this degeneracy. Interestingly, rotating the spins in state $T2$ around the (111) axis does not induce changes in the energy of the system. This is confirmed by our calculations up to an absolute error of 2 μeV. Furthermore, the energy of state $T2$ should be higher by $K_{\text{eff}}/2$ than the energy minimum of state $T1$ ($\varphi=0$). From our calculations we found this dif-

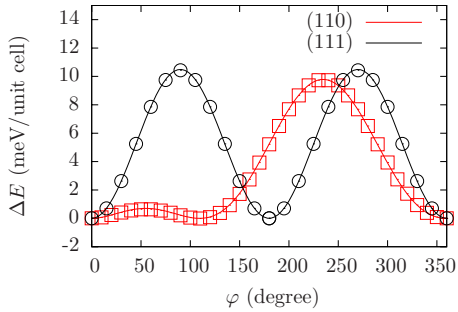

FIG. 2. (Color online) Calculated change in energy of the $L1_2$ $IrMn_3$ system when rotating the triangular $T1$ spin structure around the (111) axis (circles) and the (110) axis (squares). The solid lines display appropriate fits to $K_{\text{eff}}\sin^2(\varphi)$ and the function in Eq. (4).

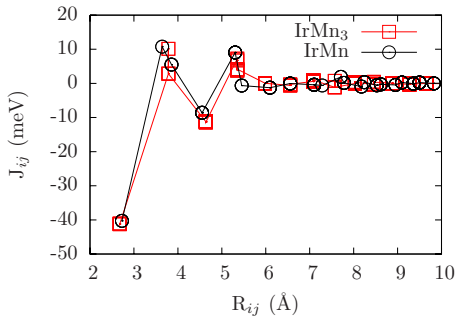

FIG. 3. (Color online) Isotropic exchange interactions J_{ij} between the Mn atoms in IrMn alloys calculated from the corresponding ground-state magnetic configurations by using the torque method (Ref. 17).

ference to be 5.22 meV, fitting nearly perfectly the previously determined MA constant.

Our last test to Eq. (1) referred to rotating the spins in state $T1$ around the (110) axis. As compared to all the previous cases, this rotation implies a quite complicated form of $E(\varphi)$,

$$E(\varphi) = E(0) + \frac{K_{\text{eff}}}{8} \times [2 + \sin^2 \varphi - 2\cos\varphi - 2\sqrt{2}\sin\varphi(1 - \cos\varphi)]. \tag{4}$$

In Fig. 2 we also plotted the results of this calculation together with the fit function as above. Reassuringly, this function describes $E(\varphi)$ well for the whole range of φ with the MA constant as obtained before (K_{eff}=10.42 meV). Note that for the rotation around the (110) axis at φ=109.47° the energy of the ground state is regained since by this rotation we obtain a $T1$ state lying in a plane normal to the $(1\bar{1}\bar{1})$ direction. In this case, we calculated an on-site anisotropy constant, $K \simeq 1.06$ meV, indicating that, unlike the $L1_0$ IrMn alloy, in this system the MAE is mainly governed by two-site anisotropy, i.e., the second term in Eq. (1).

In order to perform finite-temperature simulations on the magnetism of the IrMn compounds, we constructed a simplified effective spin model,

$$H = -\frac{1}{2}\sum_{i \neq j} J_{ij}\vec{S}_i\vec{S}_j - \frac{K_{\text{eff}}}{2}\sum_i (\vec{S}_i \cdot \vec{n}_i)^2, \tag{5}$$

where J_{ij} are isotropic Heisenberg exchange parameters and the second term on the right-hand side of Eq. (5) merges also the effect of the two-site anisotropy terms. Here, $\vec{n}_i$ are unit vectors along the local uniaxial symmetry axes. We calculated the parameters J_{ij} by using the relativistic torque method.[17,19]

For both alloys, the calculated exchange interactions are shown in Fig. 3 as a function of the distance between the Mn atoms. The two sets of interactions show obvious similarities: large antiferromagnetic (negative) nearest-neighbor interactions, sizable oscillating interactions up to about R_{ij} =6 Å, and a strong damping for larger distances. Note that double (multiple) values for some R_{ij}'s appear due to the

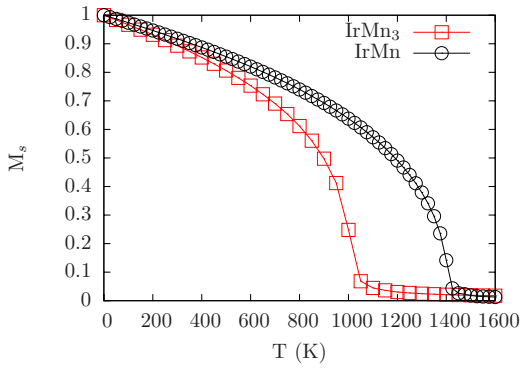

FIG. 4. (Color online) Staggered magnetizations M_s as a function of temperature obtained using Langevin dynamics over 20 ps with system sizes of 24 000 sites ($L1_2$) and 70 000 sites ($L1_0$) and using periodic boundary conditions.

different symmetry (neighborhood) of pairs with the given separation. In the case of $L1_0$ IrMn these "degeneracies" are mostly resolved via tetragonal distortion of the lattice. In good comparison with other theoretical works[13,15] from the calculated J_{ij}'s the mean-field estimates for the Néel temperatures T_N=1398 and 1222 K can be obtained.

Model (5) is simulated by solving the Landau-Lifshitz-Gilbert (LLG) equation with Langevin dynamics, calculating thermal equilibrium properties in the long-time (and high-damping) limit. The methods we use are described in detail in Ref. 20. The main quantity of interest is the sublattice staggered magnetization M_s, defined as

$$M_s = \frac{1}{n}\sum_{a=1}^{n} \langle \sqrt{M_{ax}^2 + M_{ay}^2 + M_{az}^2} \rangle, \tag{6}$$

where $\vec{M}_a = \Sigma_{i \in a}\vec{S}_i$ is proportional to the magnetization of sublattice a, n is the number of antiferromagnetic sublattices, and $\langle\ \rangle$ denotes a thermal average.

Figure 4 shows the order parameter M_s versus temperature T. Despite finite-size effects, T_N can be estimated as 1360 K for $L1_0$ IrMn and 1005 K for $L1_2$ $IrMn_3$. Note that though the exchange parameters in both cases have similar values, the critical temperature in the $L1_2$ phase is significantly lower. Obviously, the frustration of the spin ordering in the $L1_2$ phase leads to a reduced T_N as compared to the $L1_0$ phase. The simulated critical temperatures clearly improve upon the mean-field estimates as compared with experimentally observed Néel temperatures, 1145 and 960 K,[14] respectively.

A further analysis of the sublattice magnetization vectors reveals the magnetic ground-state configurations. In the case of $L1_0$ IrMn the Mn spins align along the (110) direction appropriate with the easy-plane anisotropy for this material. For the $L1_2$ system, magnetic anisotropy included according to Eq. (5) reveals that the $T1$ ground-state structure is fixed to lie in one of the (111) planes, with each of the Mn spins directed along the corresponding $(2\bar{1}\bar{1})$ directions. These spin orientations have previously been established by neutron scattering;[14] our results for the Néel temperature and the

magnetic ground-state structures are in excellent agreement with experiments, underpinning the validity of our spin model derived from first principles.

In summary, we performed an *ab initio* study for the ordered phases of IrMn and $IrMn_3$, the most important industrial antiferromagnets. The calculated Heisenberg exchange integrals and magnetic anisotropy constants are used to construct an effective spin model which is simulated using the stochastic Landau-Lifshitz-Gilbert equation. Good agreement of the calculated Néel temperatures and magnetic ground states with experimental results confirmed the validity of our approach. Our most spectacular finding is a giant second-order magnetic anisotropy for $IrMn_3$, leading to energy barriers on the order of $K_{\text{eff}} \simeq 3 \times 10^8$ erg/cc for rotation of the $T1$ ground-state spin structure around the (111) axis. This uniaxial magnetic anisotropy is understood due to the fact that the cubic symmetry is locally broken for each of the three sublattices of the antiferromagnetic $T1$ ground state.

The extremely high anisotropy for the $L1_2$ phase has perhaps not been measured experimentally because of the disordered nature of this material in thin-film devices, where deposition by sputtering causes significant loss of long-range crystallographic order. Since chemical disorder is known to drastically reduce the MAE,[21] it is not surprising that the experimentally measured MAE (Ref. 5) for granular thin films is about 1 order less in magnitude than calculated from first principles for the bulk material. Our results, therefore, suggest that finer control of the crystallography, i.e., applying growth conditions that reduce the degree of disorder, will allow the extremely large anisotropy of these materials to be fully exploited, allowing, for example, antiferromagnet film thicknesses to be reduced without loss of exchange-bias stability.[22]

Financial support was provided by the Hungarian National Scientific Research Foundation (Contracts No. K68312, No. F68726, and No. NF61726) and by the EU via COST action P19, *Multiscale Modeling of Materials*. J.J. and U.N. acknowledge financial support by Seagate Technology.

*szunyogh@phy.bme.hu

[1] J. Nogués and I. K. Schuller, J. Magn. Magn. Mater. **192**, 203 (1999).
[2] U. Nowak, A. Misra, and K. D. Usadel, J. Magn. Magn. Mater. **240**, 243 (2002).
[3] P. Miltényi, M. Gierlings, J. Keller, B. Beschoten, G. Güntherodt, U. Nowak, and K. D. Usadel, Phys. Rev. Lett. **84**, 4224 (2000).
[4] G. Vallejo-Fernandez, L. E. Fernandez-Outon, and K. O'Grady, Appl. Phys. Lett. **91**, 212503 (2007).
[5] N. P. Aley, G. Vallejo-Fernandez, R. Kroeger, B. Lafferty, J. Agnew, Y. Lu, and K. O'Grady, IEEE Trans. Magn. **44**, 2820 (2008).
[6] L. M. Sandratskii and J. Kübler, Phys. Rev. Lett. **76**, 4963 (1996).
[7] R. Y. Umetsu, A. Sakuma, and K. Fukamichi, Appl. Phys. Lett. **89**, 052504 (2006).
[8] Y. Kota, H. Tsuchiura, and A. Sakuma, IEEE Trans. Magn. **44**, 3131 (2008).
[9] O. N. Mryasov, U. Nowak, K. Guslienko, and R. W. Chantrell, Europhys. Lett. **69**, 805 (2005).
[10] J. B. Staunton, L. Szunyogh, A. Buruzs, B. L. Györffy, S. Ostanin, and L. Udvardi, Phys. Rev. B **74**, 144411 (2006).
[11] L. Szunyogh, B. Újfalussy, and P. Weinberger, Phys. Rev. B **51**, 9552 (1995).
[12] S. H. Vosko, L. Wilk, and M. Nusair, Can. J. Phys. **58**, 1200 (1980).
[13] R. Y. Umetsu, M. Miyakawa, K. Fukamichi, and A. Sakuma, Phys. Rev. B **69**, 104411 (2004).
[14] I. Tomeno, H. N. Fuke, H. Iwasaki, M. Sahashi, and Y. Tsunoda, J. Appl. Phys. **86**, 3853 (1999).
[15] A. Sakuma, K. Fukamichi, K. Sasao, and R. Y. Umetsu, Phys. Rev. B **67**, 024420 (2003).
[16] K. Selte, A. Kjekshus, A. F. Andresen, and W. B. Pearson, Acta Chem. Scand. (1947-1973) **22**, 3039 (1968).
[17] L. Udvardi, L. Szunyogh, K. Palotás, and P. Weinberger, Phys. Rev. B **68**, 104436 (2003).
[18] H. J. F. Jansen, Phys. Rev. B **59**, 4699 (1999).
[19] A. I. Liechtenstein, M. I. Katsnelson, V. P. Antropov, and V. A. Gubanov, J. Magn. Magn. Mater. **67**, 65 (1987).
[20] U. Nowak, in *Micromagnetism*, Handbook of Magnetism and Advanced Magnetic Materials Vol. 2, edited by H. Kronmüller and S. Parkin (Wiley, Chichester, 2007), pp. 858–876.
[21] J. B. Staunton, S. Ostanin, S. S. A. Razee, B. L. Györffy, L. Szunyogh, B. Ginatempo, and E. Bruno, J. Phys.: Condens. Matter **16**, S5623 (2004).
[22] M. Tsunoda, K. Imakita, M. Naka, and M. Takahashi, J. Magn. Magn. Mater. **304**, 55 (2006).